


RESEARCH ARTICLE

High salt diet-induced proximal tubular phenotypic changes and sodium-glucose cotransporter-2 expression are coordinated by cold shock Y-box binding protein-1

Anja Bernhardt¹ | Saskia Häberer¹ | JingJing Xu¹ | Hannah Damerau¹ | Johannes Steffen¹ | Charlotte Reichardt¹ | Katharina Wolters¹ | Hannes Steffen¹ | Berend Isermann² | Katrin Borucki² | Nadine Artelt^{3,4} | Nicole Endlich^{3,4}  | Renata Kozyraki⁵ | Sabine Brandt¹ | Jonathan A. Lindquist¹ | Peter R. Mertens¹

¹Clinic of Nephrology and Hypertension, Diabetes and Endocrinology, Otto-von-Guericke University Magdeburg, Magdeburg, Germany

²Institute of Clinical Chemistry and Pathobiochemistry, Otto-von-Guericke University Magdeburg, Magdeburg, Germany

³Institute of Anatomy and Cell Biology, University Medicine Greifswald, Greifswald, Germany

⁴NIPOKA GmbH, Greifswald, Germany

⁵Centre de Recherche des Cordeliers, INSERM, UMRS-1138, Université de Paris, Paris, France

Correspondence

Peter R. Mertens, Clinic of Nephrology and Hypertension, Diabetes and Endocrinology, Otto-von-Guericke University Magdeburg, Leipziger Strasse 44, 39120 Magdeburg, Germany. Email: peter.mertens@med.ovgu.de

Funding information

This work was funded by the Deutsche Forschungsgemeinschaft (DFG, German Research Foundation)—Project-ID 97850925—SFB 854: PRM (Project A01), BI (Project B26N) GRK 2408, project 7 to BI, project 8 to PRM, grants ME-1365/7-2 and ME-1365/9-2 to PRM and LI-1031/4-1 to JAL, also by the federal state Saxony-Anhalt and the European Structural and Investment Funds (ESF, 2014-2020), project number ZS/2016/08/80645

Abstract

High salt diet (HSD) is a hallmark of blood pressure elevations, weight gain and diabetes onset in the metabolic syndrome. In kidney, compensatory mechanisms are activated to balance salt turnover and maintain homeostasis. Data on the long-term effects of HSD with respect to tubular cell functions and kidney architecture that exclude confounding indirect blood pressure effects are scarce. Additionally we focus on cold shock Y-box binding protein-1 as a tubular cell protective factor. A HSD model (4% NaCl in chow; 1% NaCl in water) was compared to normal salt diet (NSD, standard chow) over 16 months using wild type mice and an inducible conditional whole body knockout for cold shock Y-box binding protein-1 (BL6J/N, *Ybx1*). HSD induced no difference in blood pressure over 16 months, comparing NSD/HSD and *Ybx1* wild type/knockout. Nevertheless, marked phenotypic changes were detected. Glucosuria and subnephrotic albuminuria ensued in wild type animals under HSD, which subsided in *Ybx1*-deficient animals. At the same time megalin receptors were upregulated. The sodium-glucose cotransporter-2

Abbreviations: ACR, albumin-to-creatinine ratio; AQP1, Aquaporin-1; AQP2, Aquaporin-2; BP, blood pressure; CA II, carbonic anhydrase II; DBP, diastolic blood pressure; ENAC, epithelial Na⁺ channel; FSD, filtration slit density; GFR, glomerular filtration rate; HSD, high salt diet; IC, intercalated cells; IMCD, inner medullary collecting ducts; IRI, ischemia-reperfusion injury; NHE3, sodium hydrogen exchanger 3; NSD, normal salt diet; OMCD, outer medullary collecting ducts; PC, principle cells; PEMP, podocyte exact morphology measurement procedure; PPAR δ , receptor peroxisome proliferator-activated receptor δ ; SBP, systolic blood pressure; SGLT2, sodium-glucose cotransporter-2; UPR, unfolded protein response; *Ybx1*, Y-box binding protein-1.

Anja Bernhardt and Saskia Häberer contributed equally to this study.

This is an open access article under the terms of the Creative Commons Attribution-NonCommercial-NoDerivs License, which permits use and distribution in any medium, provided the original work is properly cited, the use is non-commercial and no modifications or adaptations are made.

© 2021 The Authors. *The FASEB Journal* published by Wiley Periodicals LLC on behalf of Federation of American Societies for Experimental Biology

to PRM as well as by the BMBF (Bundesministerium für Bildung und Forschung) STOP-FSGS 01GM1518B to NE

(SGLT2) was completely downregulated in wild type HSD animals that developed glucosuria. In *Ybx1* knockouts, expression of AQP1 and SGLT2 was maintained under HSD; proximal tubular widening and glomerular tubularization developed. Concurrently, amino aciduria of neutral and hydrophobic amino acids was seen. In vitro translation confirmed that YB-1 translationally represses *Sglt2* transcripts. Our data reveal profound effects of HSD primarily within glomeruli and proximal tubular segments. YB-1 is regulated by HSD and orchestrates HSD-dependent changes; notably, sets reabsorption thresholds for amino acids, proteins and glucose.

KEYWORDS

cold shock protein, high salt diet, sodium glucose transporter, tubular damage

1 | INTRODUCTION

Sodium, the major extracellular cation, is essential for cellular function by controlling water distribution, electrolyte balance, and osmotic pressure.¹ For arterial hypertension, affecting 25% of adults, excessive sodium intake is a key factor.² Health organizations agree that the average daily salt (sodium chloride) consumption per person is almost double the recommended amount.³ A high salt intake is associated with adverse health outcomes, for example, increased blood pressure (BP).⁴ In addition to BP, high salt influences the immune system, leads to cardiovascular disease and delays wound healing.⁵ Furthermore, salt may play an essential role in the progression of chronic kidney disease (CKD), which is characterized by decreased glomerular filtration rate (GFR), albuminuria as well as glomerular and tubulointerstitial fibrosis, both linked with BP-dependent and -independent pathomechanisms.^{6–8} Conversely, dietary salt restriction reduces BP, albuminuria and kidney fibrosis.⁹ The effects of salt mediated by BP are well established, but almost no information is available for high salt diet (HSD)-dependent, BP-independent kidney disease. The lack of such studies is the more remarkable, since the kidney is the major organ of salt excretion and retention; and plays a key role in maintaining the sodium balance. It efficiently excretes sodium in response to high dietary intake and salvages sodium when dietary intake is low. Approximately 60%–70% of sodium reabsorption occurs via co-transporters in the proximal tubule, along with organic molecules (amino acids, glucose and organic acids).¹⁰

Previously, we identified Y-box binding protein-1 (YB-1) as a key tubular protection protein in ischemia-reperfusion injury (IRI).¹¹ YB-1 reportedly stabilizes human prorenin transcripts and regulates renin expression.¹² YB-1 is a nucleic acid chaperone and participates in most DNA- and RNA-dependent processes, including

Significance

High sodium intake provokes sodium and glucose excretion via the SGLT2 within the kidney. Here, we identify in mice a molecular link between a high salt long-term diet and kidney damage, characterized by glucosuria and proteinuria. The underlying pathomechanism is independent from blood pressure changes and relates to evolutionarily conserved cold shock proteins that regulate SGLT2 expression in tubular cells. Our study provides novel insight into the complex events initiated by a high salt ingestion and points to the phenomenon of glomerular tubularization in conjunction with tubular cell functions.

transcription, mRNA splicing and translation.^{13,14} Hence, YB-1 is essential for embryogenesis; *Ybx1* knockouts die at day E18.5.^{15,16} Here, we generated the first inducible conditional whole body murine knockout of *Ybx1* and intervened in wild type and knockout animals with a HSD to test the long-term consequences of salt intake on tubular cell phenotypes.

2 | MATERIALS AND METHODS

2.1 | Animals

The *Ybx1* gene on chromosome 4 comprises 8 exons. Exon 3 was flanked with *loxP* sites, targeting it for deletion. The Cre recombinase fused with the estrogen receptor (ERT) was placed under the control of the ubiquitous ROSA26 promoter. Activation was achieved by tamoxifen gavage inducing cleavage of the *loxP* sequences; thereby

deleting exon 3. This results in a “loss of function” mutation that induces a frame shift in exons 4 to 8, such that translation cannot take place.¹⁷ The controls are YB-1^{flox/flox} mice (C57BL/6N, Taconic) and WT^{RosaERTCre} mice (C57BL/6J, Jackson Laboratories); hereafter referred to as WT. Tamoxifen tablets were ground and dissolved overnight in ClinOleic (2 mg Tamoxifen/200 µl ClinOleic). Tamoxifen solution (200 µl/mouse) was administered via oral gavage to 8–10 weeks old animals of both sexes. Animals were maintained according to the FELASA guidelines (*Federation of European Laboratory Animal Science Association*) in a 12 h/12 h light dark cycle at 22°C in the Animal Facility of the Otto-von-Guericke University Magdeburg under specific pathogen-free (SPF) conditions using individual ventilated cages (Techniplast, Buguggiate, Italy) with free access to food and water. All procedures were conducted in accordance with the German National Guidelines for the Use of Experimental Animals (Animal Protection Act) and approved by the State of Saxony-Anhalt (AZ UniMD 42502-2-1293).

2.2 | Genotyping

Tail biopsies were lysed with 100 µl of lysis buffer (containing 50 µg of proteinase K). PCR primer pairs for mouse are listed in Table 1. Rosa26Cre PCR: 35 cycles at 95°C for 30 s, 67°C for 30 s, and 72°C for 120 s, the Rosa26Cre-WT PCR 45 cycles at 95°C for 30 s, 15 cycles at 61°C, 58°C, 55°C for 30 s, 45 cycles at 72°C for 120 s and conditional YB-1 PCR: 35 cycles at 95°C for 30 s, 60°C for 30 s, and 72°C for 60 s.

Validation of Cre recombination was performed using the conditional YB-1 forward primer and an intron 3 specific reverse primer (ACACTCCAGTCCCAGTGAAAA) under the following conditions: 30 cycles at 95°C for 30 s 58°C for 30 s, and 72°C for 3 min. Products were separated on 1% agarose-DNA stain G gels (Serva, Heidelberg, Germany). The expected sizes are 821 base pairs (bp) for full length and 345 bp for the deletion (YB-1^{ΔRosaERT}).

TABLE 1 Polymerase chain reaction primer sequences

Allele	Primer name	Primer sequence
Rosa26Cre	Cre-1	GCCTGCATTACCGGTTCGATGCAACGA
	Cre-2	GTGGCAGATGGCGCGCAACACCATT
RosaWT	fwd	CTGTGGACAGAGGAGCCATAACTGC
	rev	CCACCACTGGCTGGCTAAACTCT
Ybx1 ^{flox}	4954_133	GCCTAAGGATAGTGAAGTTTCTGG
	4954_134	CCTAGCACACCTTAATCTACAGCC
Sglt2	fwd	ATGGAGCAACACGTAGAGGC
	rev	ATGACCAGCAGGAAATAGGCA

2.3 | Sodium-rich diet

Mice were randomly assigned to a HSD (sodium-rich chow containing 4% NaCl (ssniff, Germany) and tap water containing 1% NaCl) or NSD (standard chow (ssniff, Germany) and tap water) *ad libitum*.

2.4 | Blood pressure

Blood pressure was measured non-invasively in mice using CODA[®] tail-cuff system (Kent Scientific) as described.¹⁸

2.5 | Urine measurements

Urine was collected individually in metabolic cages (Techniplast). For this, the mice were placed in cages for 24 h with access to pelleted feed and fresh water *ad libitum*, and the urine samples taken upon removal. The metabolic parameters (urine volume, glucosuria, and proteinuria) were measured before tamoxifen induction, 4 weeks after tamoxifen, and after 1, 3, 6, and 12 months on the respective diets. After collection, the urine samples were centrifuged (1500×g/min, 10 min) and the volume determined. Subsequently, the glucose and protein content were determined using NobiStrip U10 test stripes (HI-309-38810601, Hitado) according to the manufacturer's instructions. For determining blood glucose levels, mice were fasted for 4 h^{19,20} with water *ad libitum*, blood samples were taken by puncture of a tail vein and immediately analyzed using Accu-Chek Aviva Connect (PZN 11532906, Roche Diabetes Care). The concentrations of the urinary electrolytes (sodium, chloride, glucose, and urea) as well as the osmolality were measured according to the manufacturer's instructions (Roche Diagnostics, Cobas c501 module). Creatinine was determined using an enzymatic assay (Roche Diagnostics, Cobas c501 module). At the end of the intervention period (12 month), mice were sacrificed. Body weight of

the mice was assessed using a laboratory scale. Tissue samples were removed, snap frozen, and stored at -80°C until use; the second kidney was embedded for immunohistochemistry.

2.6 | Metabolomic analysis

Fresh urine samples were collected using individual metabolic cages (Tecniplast). Quantitative analysis of amino acids in urine was performed using the Amino Acid Analyzer Serie Biochrom 30⁺ according to the manufacturer's instructions (Biochrom 30⁺ Amino Acid Analyzer). Values were normalized to creatinine.

2.7 | Blood count

Blood samples were measured before induction of the YB-1 knockout, 4 weeks after induction, and after 1, 3, 6, and 12 months on the respective diets. Blood samples were subjected to complete blood cell counting (ADVIA 120; Bayer Diagnostics Munich, Germany). Serum samples were snap frozen and stored at -80°C until further analysis.

2.8 | Transcutaneous measurement of glomerular filtration rate (GFR)

GFRs were measured in mice after 16 months on the respective diets via the transcutaneous clearance of FITC-Sinistrin using a NIC-Kidney device (Mannheim Pharma & Diagnostics GmbH, Mannheim, Germany). The animals were anesthetized and the miniaturized fluorescence detector (NIC-Kidney; Mannheim Pharma & Diagnostics GmbH, Mannheim, Germany) attached to a depilated region on the back of the mice using a double-sided adhesive patch and adhesive tape. The measurement started with activation of the device before FITC-Sinistrin (70 mg/kg b.w., Mannheim Pharma & Diagnostics GmbH, Mannheim, Germany) was injected into the tail vein, in order to establish the background signal. The data acquisition lasted 120 min from the moment of injection. At the end of the 2 h recording period, mice were anesthetized and the device removed. The data were subsequently analyzed using NIC-Kidney device partner software (MPDlab v1.0, Mannheim Pharma & Diagnostics GmbH). The half-life ($t_{1/2}$) of the FITC-Sinistrin was used to calculate the GFR using the formula $\text{GFR} (\mu\text{l}/\text{min per } 100 \text{ g b.w.}) = 14616.8 \mu\text{l}/100 \text{ g b.w per half-life of FITC-Sinistrin (min)}$.²¹

2.9 | Tissue lysate preparation and Western blot analysis

Kidney tissue was mechanically homogenized in RIPA buffer (50 mM Tris-HCl, 150 mM Nonidet P-40, 1 mM sodium deoxycholate, 1 mM EDTA, and 1 mM sodium orthovanadate) containing complete protease inhibitor cocktail (Roche) at 4°C for 15 min. Protein contents were determined using the Bio-Rad protein assay (Bio-Rad, Munich, Germany). Denatured protein samples were separated using 10% SDS-PAGE and blotting onto nitrocellulose membranes. The membranes were blocked with 5% dry milk in TBS/Tween and incubated with primary antibodies diluted in TBS/T overnight at 4°C . The following antibodies were used: anti-YB-1_{C-terminal} (Y0396, Sigma), anti-DbpA (EP052151, Eurogentec), anti-AQP1 (Aquaporin-1) (AQP11-A, Alpha Diagnostic), anti-AQP2 (Aquaporin-2) (ab199975, Abcam), anti-alpha-ENaC (PA5-96353, ThermoFisher Scientific), anti-gamma-ENaC (PA5-77797, ThermoFisher Scientific), anti-CAII (Carbonic Anhydrase II) (ab191343, Abcam), anti-PERK (3192, Cell Signaling), anti-ATF-4 (11815, Cell Signaling), anti-ATF-6 (65880, Cell Signaling), anti-XBP-1s (658802, Biologend), anti- α -Tubulin (T5168, Sigma), anti-Vinculin (V284, Santa Cruz), anti-GAPDH (14C10, Cell Signaling). This is followed by incubation with the secondary, HRP-conjugated goat anti-rabbit IgG (Biozol) or goat anti-mouse IgG (Biozol) for 30 min. Following additional washing steps SuperSignal chemiluminescence substrate Pierce ECL (Thermo Scientific) was added and emitted light measured using an Intas imaging system.

2.10 | Determination of plasma renin activity

Whole blood samples were centrifuged (1500 \times g, 10 min, at room temperature) and the supernatant (i.e., plasma) collected. Protease inhibitor (PMSF) was added to the plasma sample (1:100). Two aliquots (50 μl each) were incubated (one at 0°C and the other at 37°C) and subsequently assayed using the angiotensin I plasma renin activity ELISA (IBL international, Hamburg, Germany), according to the manufacturer's instructions.

2.11 | Immunohistochemistry

Formalin-fixed, paraffin-embedded tissue sections were used for immunohistochemistry (avidin-biotin complex (ABC) method) and immunofluorescence staining. For SGLT2 (sodium-glucose cotransporter 2), megalin,

cubulin, NHE3 (sodium hydrogen exchanger 3), renin, YB-1, AQP1, AQP2 and CA II (Carbonic Anhydrase II) staining, 10 mM sodium citrate buffer (pH 6.0) was heated in the microwave for 5 min. Endogenous peroxidase was inactivated by incubation in 3% hydrogen peroxide. After washing, the sections were incubated with blocking solution (10% FCS, 1% BSA in 1× Tween-PBS) for 30 min at room temperature and incubated overnight at 4°C with the primary antibody (mouse renin antibody, R&D Systems, AF4277, 1:400; SGLT2, Abcam, ab37296, 1:200; NHE3, Novusbio, NBP1-82574, 1:1000; AQP2, Santa Cruz, sc-515770, 1:50; CA II, Abcam, ab191343, 1:50; AQP1, Santa Cruz, sc-25287, 1:300) diluted in 1% FCS plus 1× Tween-PBS. Primary antibodies for megalin and cubulin used were sheep anti-rat megalin and rabbit anti-rat cubulin.²² After incubation with peroxidase-labeled secondary antibody (Jackson Immuno Research, 705-035-147, 1:500) for 1 h at room temperature, sections were developed using diaminobenzidine substrate and counterstained with hematoxylin solution. Subsequent dehydration was achieved by means of an ascending alcohol series (70% ethanol, 80% ethanol, 96% ethanol and 100% ethanol). Finally, washing was performed twice for 5 min in Histo-Clear® (Carl Roth, Karlsruhe, Germany). Embedding was performed with ROTI®-Histokitt II (Carl Roth GmbH, Karlsruhe, Germany) according to the manufacturer's instructions. For immunofluorescence staining, secondary antibodies conjugated with Alexa Fluor Plus 647 (Thermo Fisher Scientific), TRITC (Jackson ImmunoResearch) and Cy3 (Jackson ImmunoResearch) were used at 1:100 dilution. Coverslips were mounted using the ProLong Gold Antifade fluorescence mounting medium (Thermo Fisher Scientific) with DAPI (Vector Laboratories), and sealed using nail polish. Stained tissue sections were imaged on a Leica DM6000B microscope using Leica application suite advanced fluorescence software and ImageJ for image acquisition.

2.12 | Super resolution microscopy

Mice were sacrificed and kidney samples were embedded in paraffin. Podocyte exact morphology measurement procedure (PEMP) was performed to determine the filtration slit density (FSD) as described previously.²³ Briefly, 3 µm paraffin sections were deparaffinized, rehydrated and incubated in a pressure cooker in the presence of Tris-EDTA buffer (10 mM Trizma Base, 1.27 mM EDTA, 0.05% Tween20, pH 9.0). Sections were stained with guinea pig anti-nephrin serum (GP-N2; Progen, Heidelberg, Germany; 1:600) and finally with Cy3-labeled donkey anti-guinea pig IgG (Jackson Immuno Research, Hamburg, Germany). 3D-SIM (structured illumination microscopy)

images were acquired on a Zeiss Elyra PS.1 system (Carl Zeiss, Jena, Germany) and reconstructed using Zeiss ZEN black software. For measurement of the FSD, a custom-built Fiji plugin was used.²⁴ FSD values were calculated from 16 to 20 glomeruli of 2–3 mice per group. Two-way analysis of variance with Bonferroni correction for multiple testing was used for statistical analysis.

2.13 | Isolation of total RNA

Total RNA was extracted from kidney tissue samples using TriFast™ reagent (Peqlab, Erlangen, Germany) according to the manufacturer's instructions. RNA was reverse transcribed using Transcriptor High Fidelity cDNA kit (Roche, Mannheim, Germany). PCR was performed using the PCR Mastermix kit (Quantace, London). The standard temperature profile included initial denaturation for 3 min at 95°C, followed by 30 cycles of denaturation at 95°C for 30 s, annealing at 51.5 to 53°C (primer dependent) for 30 s, and extension at 72°C for 1 min. Products were separated on 1% agarose/ethidium bromide gels. The expected product sizes are 104 base pairs (bp) for SGLT2 (Table 1).

2.14 | In vitro translation system

Plasmids (pT7) for in vitro translation were prepared by VectorBuilder (Chicago, USA) (Supplementary Figure S7C). In vitro transcription reactions were performed according to the manufacturer's instructions in the T7 RiboMAX™ Express Large Scale RNA Production System (Promega) in a 60 µl reaction containing the following: 30 µl of RiboMAX™ Express T7 2× Buffer, 9 µl of nuclease-free water, 15 µl of SGLT2 linear template DNA (3 µg) and 2 µl of Enzyme Mix. In vitro transcription reactions were incubated at 37°C for 30 min. After removing the DNA template and unincorporated nucleotides, the RNA concentration was quantitated by ultraviolet light absorbance at a wavelength of 260 nm. In vitro translation reactions were performed according to the manufacturer's instructions in the Rabbit Reticulocyte Lysate System, Nuclease Treated (Promega). Untreated Rabbit Reticulocyte Lysate contains the cellular components for protein synthesis (tRNA, ribosomes, amino acids, initiation, elongation and termination factors). A 50 µl reaction containing the following components: 35 µl of Rabbit Reticulocyte Lysate, 0.5 µl of amino acids, 1 µl of RNasin® Ribonuclease Inhibitor, 1.5 µl FluoroTect™ tRNA Green_{Lys} tRNA, 8.4 µl of nuclease-free water and 2 µg/µl of *Sglt2* mRNA. In vitro translation reactions were incubated at 30°C for 90 min.

Recombinant human YB-1 (pcDNA3/Flag-YB-1) was a gift of K. Kohno. Flag-YB-1 was purified with

anti-DYKDDDDK G1 affinity resin (L00432, Genscript) following the manufacturer's instructions and eluted with Flag-peptide (100 µg/ml). After dialysis in polyethylene glycol solution (average molecular weight 20 kDa), purified protein was shock frozen and stored at -80°C until use.

2.15 | Statistical analysis

All results were confirmed through at least two independent experiments performed in triplicates, if not otherwise stated. Results were calculated and are presented as means \pm standard deviation (SD). Statistical analysis were performed using GraphPad™ prism 7 (GraphPad Software La Jolla, CA, USA) and two-way ANOVA followed by Sidak's multiple comparison test. The Student's t test was applied for two-group comparisons with $p < .05$ (*), $p < .01$ (**), and $p < .001$ (***) considered statistically significant.

3 | RESULTS

3.1 | The *Ybx1* knockout

Conventional *Ybx1*^{-/-} deletion is embryonic lethal,¹⁵ therefore we generated an inducible whole body knockout (*Ybx1*^{ΔRosaERT}) by crossing C57BL/6N *Ybx1*^{fllox/flox} mice with the ubiquitously expressed C57BL/6J WT^{RosaERTCre}. Genotyping confirmed the presence of both alleles (Supplementary Figure S1A) as well as successful recombination; a 345 bp

PCR product indicates deletion of exon 3 following oral tamoxifen application (Supplementary Figure S1B). All organs, except brain, show a complete knockout (Figure 1A). Absence of YB-1 protein was confirmed by Western blot (Figure 1B) and flow cytometry (Supplementary Figure S1C). We also confirmed that *Ybx1* deficiency results in embryonic lethality (Supplementary Figure S1D).

Knockout mice show comparable growth over 16 months (WT: 28.3 ± 0.4 g; *Ybx1*^{ΔRosaERT}: 29.1 ± 0.6 g; Supplementary Figure S2A). Although the classical *Ybx1* knockout is lethal, the inducible knockout appears perfectly healthy (Supplementary Figure S2B). This is unexpected due to the proliferation arrest reported after *Ybx1* knockdown.^{13,25} The only abnormality observed by histology of the *Ybx1* knockout epidermis was a markedly reduced skin thickness and altered architecture (Supplementary Figure S2E) as described by Kwon et al, however no changes in fur were visible.²⁶ Peripheral blood analyses show no differences in either the relative or absolute abundance of cells (Supplementary Table S1).

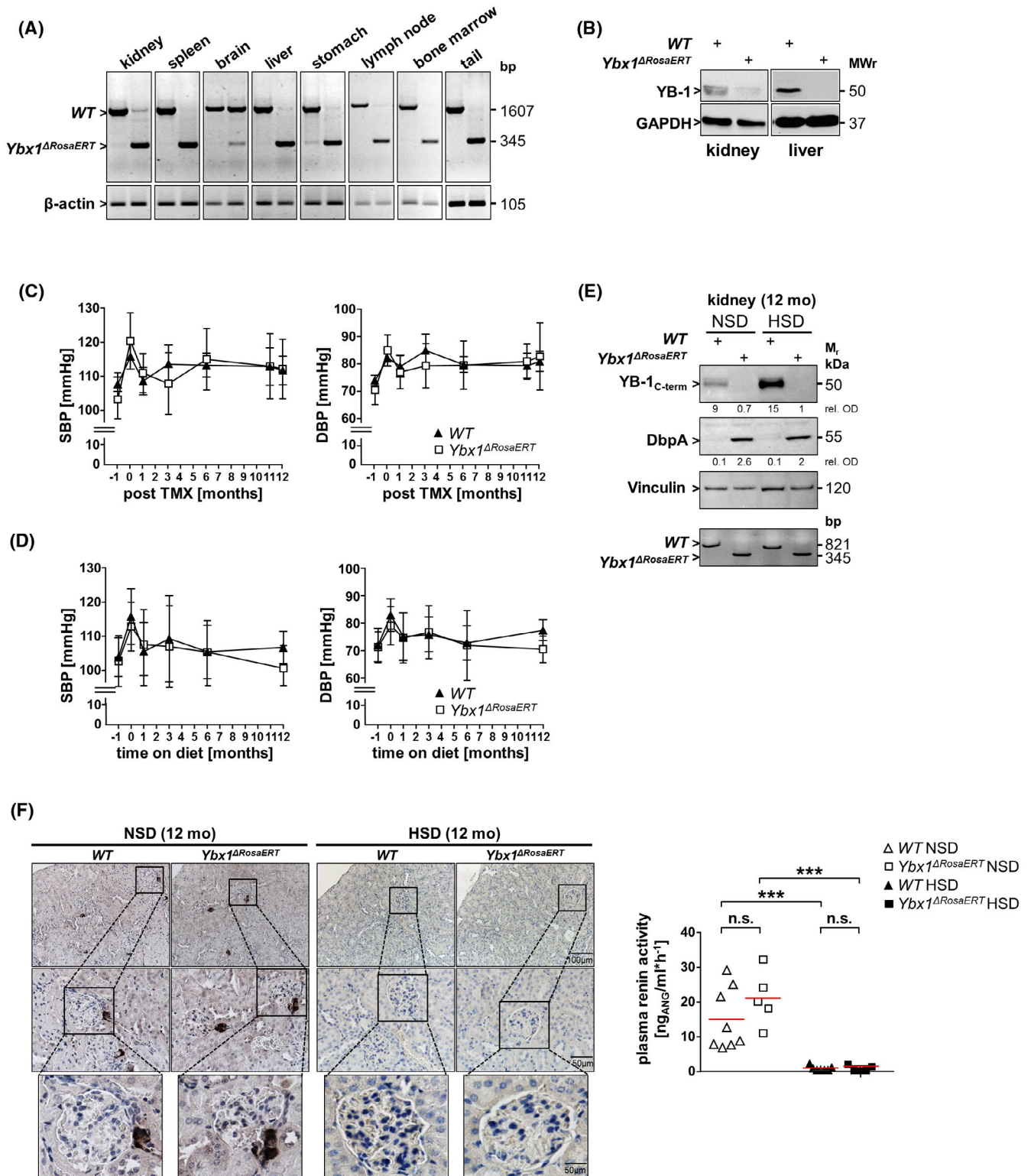
3.2 | HSD does not affect blood pressure

YB-1 reportedly stabilizes preprorenin mRNA.¹² We theorized that YB-1 loss results in fewer transcripts, less renin synthesis and therefore a drop in BP. Systolic and diastolic BP (Figure 1C; SBP/DBP) were measured regularly by tail cuff over 12 months; no differences were observed. Thus, *Ybx1* deletion does not alter BP in the murine model.

FIGURE 1 Tamoxifen application induces *Ybx1* deletion in multiple organs. (A) The whole body *Ybx1* deletion was confirmed by polymerase chain reaction (PCR) 4 weeks after tamoxifen treatment. Both WT and *Ybx1* knockout organs showed corresponding bands of 1607 bp for full length and 345 bp in *Ybx1* knockout (*Ybx1*^{ΔRosaERT}) for the PCR products from kidney, spleen, liver, stomach, lymph nodes, bone marrow, and tail. The brain PCR band shows that the *Ybx1* gene was not excised after tamoxifen treatment, as a WT band (821 bp) is still detected. The faint 345 bp band indicates only a partial activation of Cre activity in this tissue. (B) Western blot analysis of Y-box binding protein-1 (YB-1) expression in kidney and liver. WT mice exhibited the expected YB-1 protein band (50 kDa), whereas no protein is detected in *Ybx1* knockout mice. (C) Blood pressure recordings were performed at regular intervals in *Ybx1* knockout and WT animals over the 12 months observation period. There was no difference in the systolic blood pressure (SBP) or in the diastolic blood pressure (DBP) in WT versus *Ybx1* knockout (*Ybx1*^{ΔRosaERT}) animals. (D) Blood pressure measurements were also performed in *Ybx1* knockout and WT animals under high salt diet (HSD). There was no difference in SBP and DBP in WT versus knockout (*Ybx1*^{ΔRosaERT}) animals over the 12 months observation period under HSD. Therefore the HSD did not cause widespread hypertension. Data represent means \pm SD, with $n = 9$ for WT and $n = 6$ for knockouts. (E) Western blot analysis of YB-1 expression under normal and high salt conditions confirmed the absence of YB-1 protein in *Ybx1* knockout mice. YB-1 expression was induced in kidney tissues in WT mice under HSD. The loss of YB-1 induces the expression of DbpA, which is not influenced by high salt. *Ybx1* deletion was confirmed by PCR in kidney biopsies taken 12 month under HSD. The WT mice showed the expected full-length product of 821 bp, while *Ybx1* knockout mice (*Ybx1*^{ΔRosaERT}) show the expected truncated product at 345 bp, confirming Cre recombinase activity. (F) Immunohistochemical staining showed that renin positive area was larger in mice after 12 months on a normal salt diet (NSD), and positive staining was restricted to the juxtaglomerular apparatus. There was no significant difference between WT and *Ybx1* knockout mice. Representative photomicrographs of kidney tissue sections, magnification $\times 20$ (top); $\times 40$ (bottom), scale bars indicate 100; 50 µm respectively. For the animals receiving HSD, the renin staining area was smaller than in NSD. There was no significant difference between WT and *Ybx1* knockout mice. The activity of plasma renin was measured by ELISA. For the NSD there was no difference in the plasma renin activity in WT animals versus *Ybx1* knockout (*Ybx1*^{ΔRosaERT}). The plasma renin activity was significantly lower in the animals receiving the HSD regardless of the genotype. Data represent means \pm SD, $n \geq 5$ for each group, *** $p < .0005$

Cold shock proteins are upregulated by cellular stress.²⁷ Since high salt induces a systemic inflammatory milieu and hypertension,⁴ a long-term intervention was performed (Supplementary Figure S3). Similar to the NSD (Figure 1C), 12 months of HSD showed no changes in systolic and diastolic BP ($102/72 \pm 5$ mmHg vs. $105/74$

± 5 mmHg, Figure 1D). To test whether the lack of hypertension is attributed to the mixed BL6J/N background, BP recordings were performed in C57BL/6J and -N WT animals. No differences were observed (Supplementary Figure S2C,D). Thus, HSD does not induce hypertension in the chosen genetic background.



3.3 | HSD induces YB-1 expression

In WT mice under HSD YB-1 protein levels increase in kidney tissue compared to NSD (Figure 1E), indicating that sodium induces YB-1 expression. The YB-1 homolog DbpA is not detected in healthy kidney, apart from vascular smooth muscle cells.²⁸ However, DbpA expression is detected in *Ybx1* knockout animals (Figure 1E). Thus cold shock proteins show a compensatory regulation. DbpA expression is not induced by HSD. Western blot and PCR analyses of aged mice confirmed that the *Ybx1* knockout is maintained (Supplementary Figure S4A,B). HSD does not affect weight gain or mortality until 16 months (Supplementary Figure S4C,D).

3.4 | HSD suppresses renin synthesis and secretion

In healthy kidney, renin is primarily found in juxtaglomerular cells within the macula densa.²⁹ As mentioned above, the loss of YB-1 should result in reduced plasma renin levels. The distribution of renin positive cells was comparable under NSD, while a complete downregulation of renin is observed following HSD (Figure 1F). *Ybx1* deletion had no influence on plasma renin content. As expected, renin activity is significantly higher for NSD than HSD (Figure 1F). Renin and YB-1 co-staining demonstrate the absence of YB-1 protein in knockouts. In WT, YB-1 protein is detected in tubular cells and juxtaglomerular cells, where it co-localizes with renin. Semi-quantitative assessment shows no differences (Supplementary Figure S5A). Thus, these results do not indicate a regulatory effect of YB-1 on renin secretion.

3.5 | HSD and YB-1 regulate proximal tubular cell function

An overview on the key functional proteins expressed by glomerular (AQP1 and SGLT2), the proximal (albumin,

cubulin, megalin, SGLT2, sodium hydrogen exchanger 3 (NHE3), AQP1) and distal tubular cells (AQP2, CAII, epithelial Na⁺ channel (α - and γ -ENaC)) under NSD and HSD are summarized in Figure 2A. Before dietary changes, 24 h urine volumes were similar in WT and *Ybx1* knockout animals (Figure 2B). HSD significantly increased urinary output (>2 ml/day) in both groups compared to NSD mice; reaching >9 ml/day from month 6 onwards. A significant increase in urine output in WT compared to knockout animals occurred after 16 months. Notably, *Ybx1* deficiency significantly limited urinary protein excretion that is a 90% reduction in albumin-to-creatinine ratio (ACR, Figure 2C and Supplementary Figure S6A). Next we assessed the GFR (Supplementary Figure S6B) via FITC-sinistrin clearance, which did not differ between WT and knockout NSD mice, but a significantly lower GFR is seen for WT compared to knockout animals on a HSD.

At 12 months of HSD, serum osmolality shows no changes (Supplementary Figure S6C) whereas urine urea shows significant higher values in WT animals (Supplementary Figure S6D). WT mice excreted up to twice as much sodium (Figure 2D) and chloride (Supplementary Figure S6E) compared to knockouts.

Blood glucose levels are similar and not affected by HSD (Supplementary Figure S6F). Urine samples from NSD mice show similarly low glucose values, whereas urine glucose levels are significantly higher in WT than in knockout animals under HSD (Figure 2E), indicating that the glucose concentration in the primary urine exceeds the tubular reabsorption capacity.

Daily excretion rates of urinary amino acids were quantified. No differences in excretion was observed for NSD with the two genotypes (Figure 3A). However, HSD results in a marked higher excretion of neutral and hydrophobic amino acids, and to a lesser extent basic amino acids. We conclude that tubular cell stress with perturbation of transporter expression under HSD leads to amino aciduria after 12 months that is augmented by *Ybx1* deficiency. Taken together, we establish a direct role for cold shock protein YB-1 on the tubular cell phenotype and reveal a downregulation of amino acid transporters.

FIGURE 2 Urine composition is dependent on salt diet and *Ybx1* genotype. (A) The results for key functional proteins expressed by the glomerulus (aquaporin-1 (AQP1) and sodium-glucose cotransporter-2 (SGLT2)), the proximal (albumin, glucose, cubulin, megalin, SGLT2), sodium hydrogen exchanger 3 (NHE3), amino acids, (AQP1)) and distal tubular cells (aquaporin-2 (AQP2), carbonic anhydrase II (CAII), epithelial Na⁺ channel (α - and γ -ENaC)) are summarized. Urine volume, albuminuria and sodium concentration were periodically measured for both genotypes (WT controls/*Ybx1* ^{Δ RosaERT}) and treatment groups (normal salt diet, NSD; high salt diet, HSD). (B) For the animals receiving a NSD the urine output remained low. Under high salt conditions, the urine volume increased over time for all animals, regardless of the genotype (WT and *Ybx1* knockout). After 16 months of diet there was a significant increase in urine output in WT animals compared to *Ybx1* knockout. (C) For the animals receiving a NSD the urine albumin concentration remained low, irrespective of the genotype. The urine protein of WT mice under HSD increased significantly. (D) Sodium level in the urine increased significantly under HSD. WT mice excreted up to twice as much sodium compared to *Ybx1* knockout. (E) Interestingly, for WT mice receiving a HSD there was a significant increase in urine glucose level >10 mmol/L from 3 month onwards with HSD compared to the *Ybx1* knockout animals. Data represent means \pm SD, $n = 6-9$ for each group, * $p < .05$, ** $p < .005$

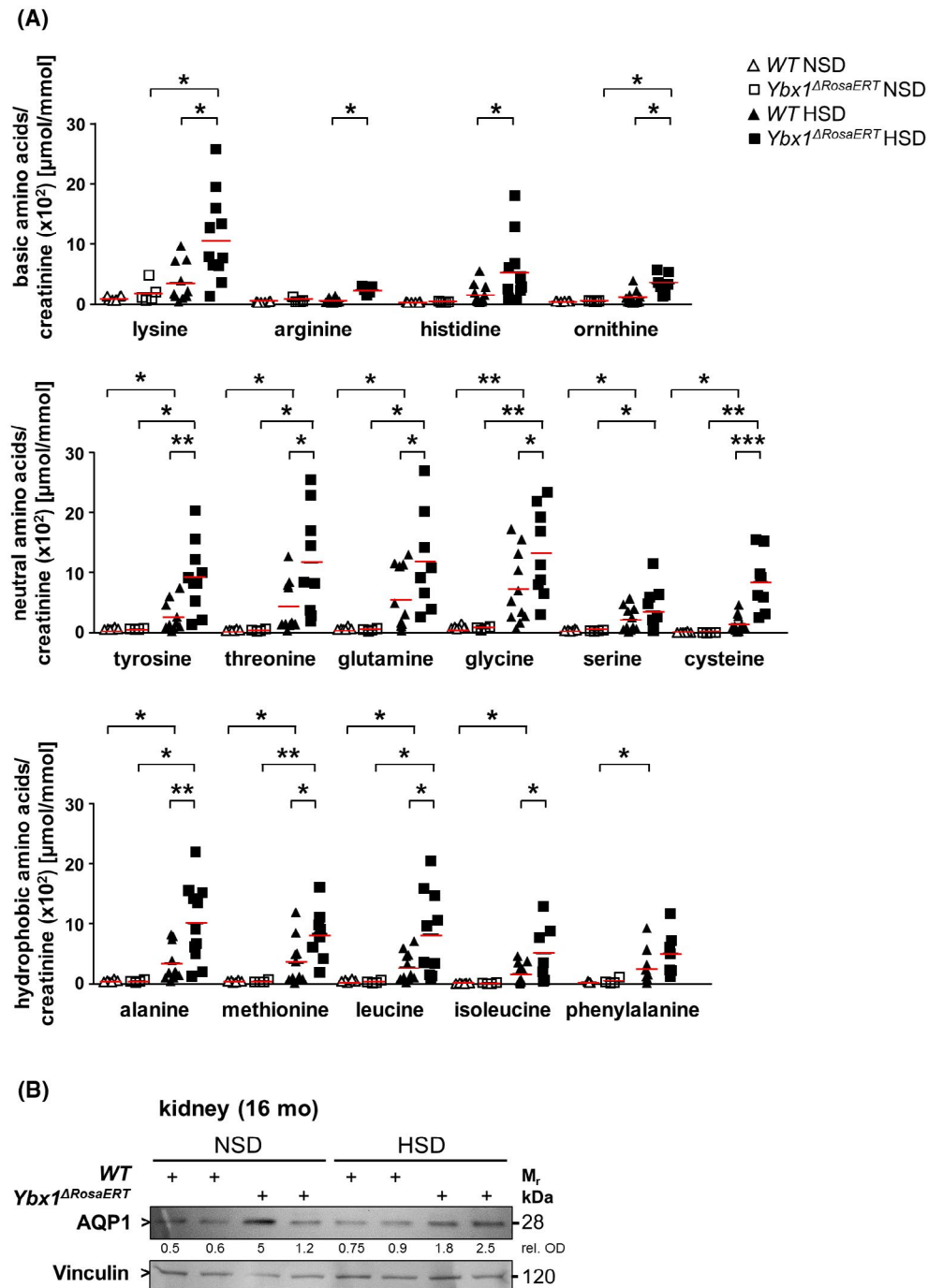


FIGURE 3 High salt diet (HSD) and *Ybx1*-deficiency upregulate amino aciduria. (A) To detect alterations in amino acid metabolism and excretion that are controlled by proximal tubular cells, quantification of basic, neutral and hydrophobic amino acids was performed in urine collections. Firstly, there was no excess excretion of amino acids in *Ybx1* knockout animals compared to WT animals on a normal salt diet (NSD). Challenge with a HSD results in a marked excretion of neutral and hydrophobic amino acids into the urine, and to a lesser extent also basic amino acids. This excretion was markedly enhanced in the *Ybx1* knockout strains. Data represent means \pm SD, $n = 10$ –12 for each group, * $p < .05$, ** $p < .005$, *** $p < .0005$. (B) Western blot analysis of aquaporin-1 (AQP1) expression under NSD and HSD conditions. AQP1 expression was reduced in kidney tissue in WT mice compared to *Ybx1* knockout animals under HSD

the tubular cell changes, immunohistochemistry was performed for key transporters of proximal and distal nephron segments. Cubulin and megalin are multi-ligand receptors that regulate receptor-mediated endocytosis.³² Cubulin shows a strong apical staining in proximal tubules of NSD

mice and enhanced expression in *Ybx1* knockout animals. HSD significantly blunted cubulin expression in WT and knockouts (Figure 4A,B). For megalin, a similar pattern is observed for NSD, with marked upregulation under HSD, particularly in *Ybx1* knockout animals (Figure 4C,D).

Thus, megalin and cubulin are differentially regulated by YB-1 under HSD. Next we examined SGLT2 expression, as it this transporter mediates more than 90% of glucose reabsorption. SGLT2 localizes to the luminal side of proximal tubules (Figure 4E). WT mice lose SGLT2 expression after short-term (6 months) and long-term (12 months) HSD, whereas *Ybx1* knockout mice show strong basolateral staining (Figure 4F, Supplementary Figure S7D). In addition, knockout tubules are dilated and cells have lost their cell junctions. Subsequently NHE3 expression, which regulates Na⁺ and water reabsorption from the filtrate, was examined.³³ NHE3 is significantly reduced in knockouts compared to WT under NSD (Figure 4G). HSD shows a strong induction of NHE3 in the cortex of both WT and knockout animals (Figure 4H). Thus, the expression of both transporters is affected by both sodium-rich diet and YB-1.

3.6 | HSD induces podocyte effacement

To test for changes in the glomerulus, specifically the composition of the filtration barrier by podocyte foot processes, 3D-structured illumination microscopy (3D-SIM) was performed to visualize the filtration slit density (FSD).²³ The FSD does not differ under NSD between both genotypes. In contrast, areas with strongly effaced foot processes are seen under HSD, irrespective of genotype (Supplementary Movie). Podocyte exact morphology measurement procedure shows significant differences in FSD under HSD (Supplementary Figure S6G, Supplementary Table S2).

To determine the role of HSD-induced stress, we analyzed the activation of the unfolded protein response in WT and *Ybx1* knockout animals (Supplementary Figure S6H). A significant reduction in total PERK, ATF-6, and in spliced XBP-1s is observed under HSD compared to NSD. In *Ybx1* knockout animals these proteins were even less abundantly expressed, indirectly indicating that YB-1 coordinates the unfolded protein response (UPR).

3.7 | Distal tubule cell reabsorption is independent of YB-1

The aldosterone sensitive principle cells (PC) are found in the late distal convoluted tubule, connecting tubule and collecting duct together with intercalated cells (IC).³⁴ PC are more common in the distal nephron and collecting duct and express two key receptors, AQP2 and ENaC, which regulate plasma osmolality, extracellular volume and water reabsorption. Based on the study by Mukherjee et al.³⁵ we investigated the composition of renal tubular epithelial cells (Figure 5A). No significant differences in

the number of PC and IC were detected (Figure 5B). ENaC allows the flow of Na⁺ ions across epithelia to maintain body salt and water homeostasis. HSD resulted in significantly increased protein expression of α - and γ -ENaC (Figure 5C), irrespective of genotype. Thus, we conclude that YB-1 is not critical for distal tubule cell reabsorption under HSD.

3.8 | SGLT2 expression is influenced by the loss of YB-1

SGLT2 expression was visualized in kidney specimens with co-staining for AQP1 as proximal tubule marker (Figure 6A). Compared to NSD SGLT2 expression is suppressed by HSD in WT animals. In contrast the transporter is markedly upregulated in *Ybx1* knockout animals under HSD, but not NSD (Figure 6B). Unexpectedly, SGLT2 expression is seen within the glomerulum in cells situated at the parietal aspect of the Bowman's capsule, suggesting glomerular tubularization (Figure 6C).³⁶ The striking overlap of AQP1 with SGLT2 reinforces the fact that these changes occur within the proximal tubule. *Sgt2* transcripts showed no difference in absolute numbers (Figure 6D), suggesting that YB-1 translationally represses this mRNA. Sequence analysis identified 21 potential YB-1 binding sites (Supplementary Figure S7A,B). In vitro translation experiments show that recombinant YB-1 inhibits translation of a model transcript harboring these motifs, confirming the proposed model of translational regulation (Figure 6E).

3.9 | HSD and YB-1 regulate immune cell infiltration

Infiltrating numbers of circulating and kidney tissue infiltrating leukocytes were quantified. The results indicate that HSD transiently increases eosinophil numbers in the blood circulation, which was seen with both genotypes at time point 3 months. The differences however subsided following 6 month. The total number of circulating leukocytes did not change with the different diets and genetic backgrounds (Supplementary Figure S8A). Regarding immune cell infiltration of kidney tissue we performed additional experiments by staining for CD45⁺ leukocytes and F4/80⁺ macrophages using immunofluorescence microscopy (CD45 stained in red, F4/80 stained in green; Supplementary Figure S8B). As expected, only a low number of cells are positive for CD45 in kidneys from animals receiving NSD. A high salt intake was accompanied by increased influx of immune cells into the kidneys of WT mice (leukocytes and macrophages after 12 months). In

contrast the *Ybx1* knockout animals exhibited less kidney infiltrates of CD45⁺ and F4/80⁺ cells under HSD. This indicates that *Ybx1* knockout is accompanied by a blunted inflammatory response, linking YB-1 expression with high salt effects.

4 | DISCUSSION

It is undisputed that high salt ingestion may result in elevated blood pressure; however, this response is not uniformly seen and salt-sensitive as well as insensitive patients may be identified.³⁷ Animal studies have tried to recapitulate the human situation with different setups. Dietary salt overload contribute to renal injury documented by albuminuria and decreased GFR.⁴ Most previous findings were designed with short-term sodium loading of mice or rats and analyses on fluid and salt homeostasis as well as organ damage.^{38–40} The first study describing an ultra-long-term exposure in salt intake has been published in 2015, demonstrating elevated blood pressure, increase of sodium excretion and higher steroid hormone levels.^{41,42} Further findings have demonstrated that a high salt intake can adversely affect target organs, including stiffening of blood vessels.³⁷ The elevated blood pressure closely linked with high salt ingestion confounds findings in most models, given the detrimental effects of high blood pressure on the heart, kidneys, vessel alterations, amongst others. In our chosen animal model the genetic background C57BL/6J and -N is likely the reason for unaltered blood pressure recordings in the different groups. There are contradictory reports on the sensitivity of C57BL/6 mice to salt with regard to hypertension, with different studies reporting positive and some reporting neutral findings.⁴³ In a study from Yu et al after 8% HSD the C57BL/6J mice exhibited arterial hypertension with an increase of 33% in maximum systolic pressure and a decrease of 44% in arterial elasticity.⁴⁴ Under these

conditions one may not unequivocally determine whether cold shock protein YB-1 is relevant for blood pressure regulations via renin transcript regulation, as previously reported.¹² At least from the results obtained with serum renin concentrations and activities there were no differences with genetic *Ybx1* depletion. Given the matching blood pressure recordings over the whole experimental setup of 16 months the animals however provide a unique opportunity to determine kidney damage with excessive sodium loading that are independent from BP changes. Our findings are in line with previous studies showing albuminuria⁴⁵ and a decline in GFR.⁴⁶

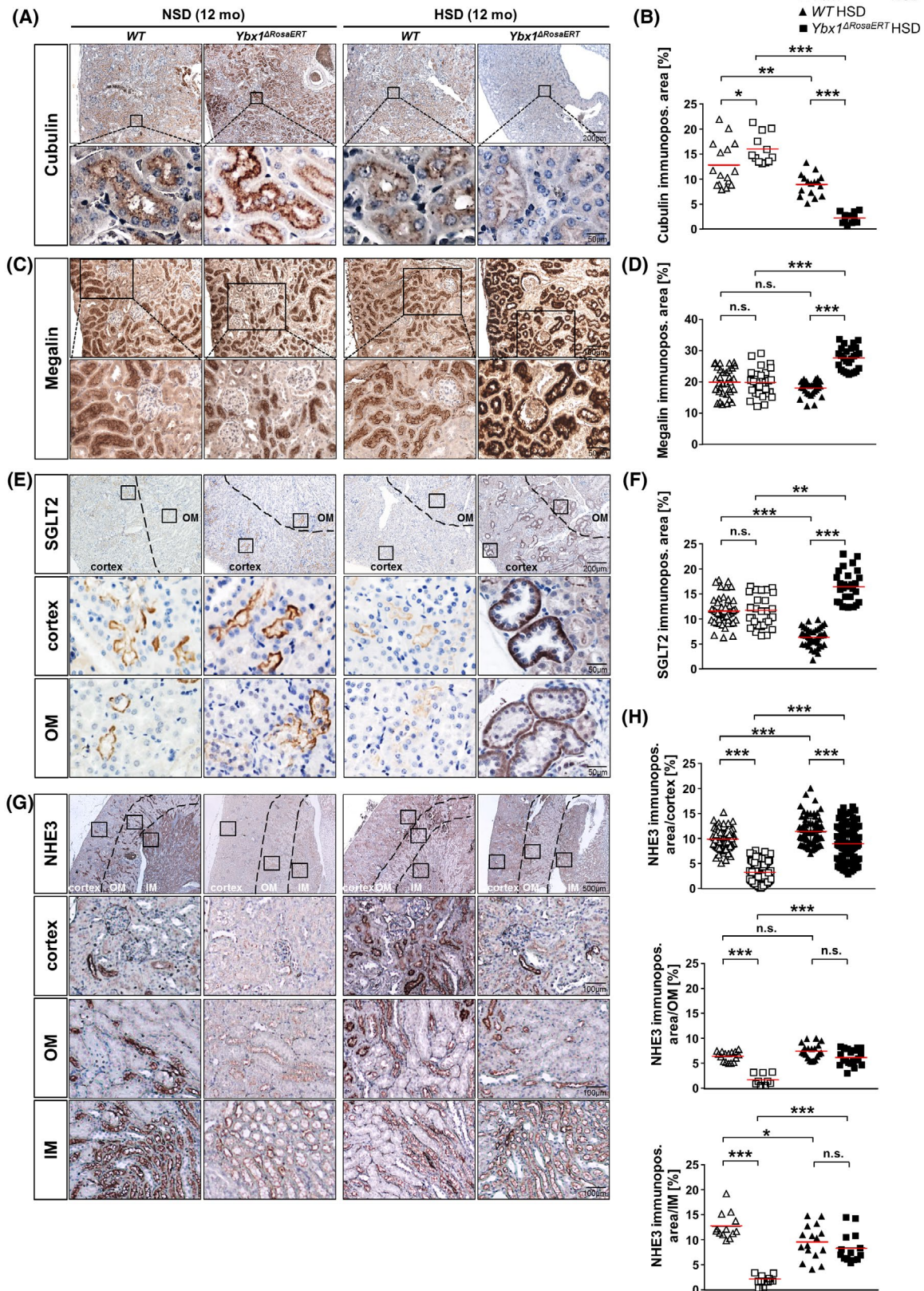
Over time proteinuria and glucosuria developed, without evidence of a diabetic metabolism. These changes started at the same time around 3 months and were linked with prominent phenotypic changes of tubular cells in the proximal tubules. Furthermore, subtle changes were detected for the podocyte foot processes with effacement under HSD at time point 12 months.

To provide insight into the pathomechanisms underlying HSD-related proteinuria, megalin and cubulin expression were analyzed. Our data show that increased urinary protein excretion in WT HSD mice may be linked to the downregulation of cubulin.⁴⁷ Decreased cubulin and megalin expression has been shown in diseases that are characterized by proteinuria and defective proximal tubule endocytosis.⁴⁸ On the other hand, we see that *Ybx1* deletion prevents HSD-induced proteinuria, which is associated with increased megalin expression and enhanced amino acid excretion. This adaption may reduce urinary protein loss in knockout HSD mice. Interestingly, the pattern of megalin expression in knockouts differs from that of cubulin, suggesting that megalin and cubulin are differentially regulated. The depletion of *Ybx1* markedly affects receptor expression and links *Ybx1* deficiency with tubular cell functions. Previously, we identified a cytoprotective effect for YB-1 following IRI in *Ybx1*^{+/-} kidneys.¹¹ Here, we demonstrate that *Ybx1* deficiency does not

FIGURE 4 The deletion of *Ybx1* markedly affects proximal tubular function. (A) In mouse tissue, the cubulin expression in the proximal tubule is enhanced in *Ybx1* knockout mice, which is ablated by challenge with a high salt diet (HSD). (B) Quantification of cubulin stained tissue area [%]. (C) Immunohistochemistry shows that there is no difference in megalin positive area between WT and *Ybx1* knockout mice fed with normal salt diet (NSD). However, the megalin positive area increases in *Ybx1* knockout mice after 12 months on a high salt diet (HSD). Representative photomicrographs of kidney tissue sections, magnification ×10 (top cubulin); ×20 (top megalin); ×40 (bottom), scale bars indicate 200; 100; 50 μm respectively. (D) Quantification of megalin stained area [%]. (E) Kidney sections were stained for sodium-glucose cotransporter-2 (SGLT2). Under a HSD, SGLT2 protein level as determined by IHC is strongly increased in *Ybx1* knockout mice on the basolateral side of the tubule, whereas WT mice appear to lose SGLT2 expression. Representative micrographs of kidney tissues from WT and *Ybx1* knockout mice under NSD and HSD. Magnification ×10; ×40, scale bars indicate 200; 50 μm respectively. (F) Quantification of SGLT2 stained area [%]. (G) Immunohistochemistry shows that the sodium hydrogen exchanger 3 (NHE3) positive area is reduced in *Ybx1* knockout mice after 12 months on a NSD. An induction of NHE3 expression under a HSD is seen within the cortex and a restored expression in the inner medulla of *Ybx1* knockout mice. Representative photomicrographs of kidney tissue sections, magnification ×5 (top); ×20 (bottom), scale bars indicate 500; 100 μm respectively. (H) Quantification of NHE3 stained tissue [%]. The tubule and its surrounding positive staining fractions were analyzed using ImageJ software, with at least four mice per group. Data represent means ± SD, *n* = 4 for each group

protect against high salt-induced damage. There are however numerous differences between the two models and reports. First, the YB-1 content of *Ybx1*^{+/-} mice is 50%,

whereas *Ybx1*-deficient animals have none. Secondly, IRI is a rapid model that induces acute injury, whereas HSD, applied over months, represents cumulative damage. We



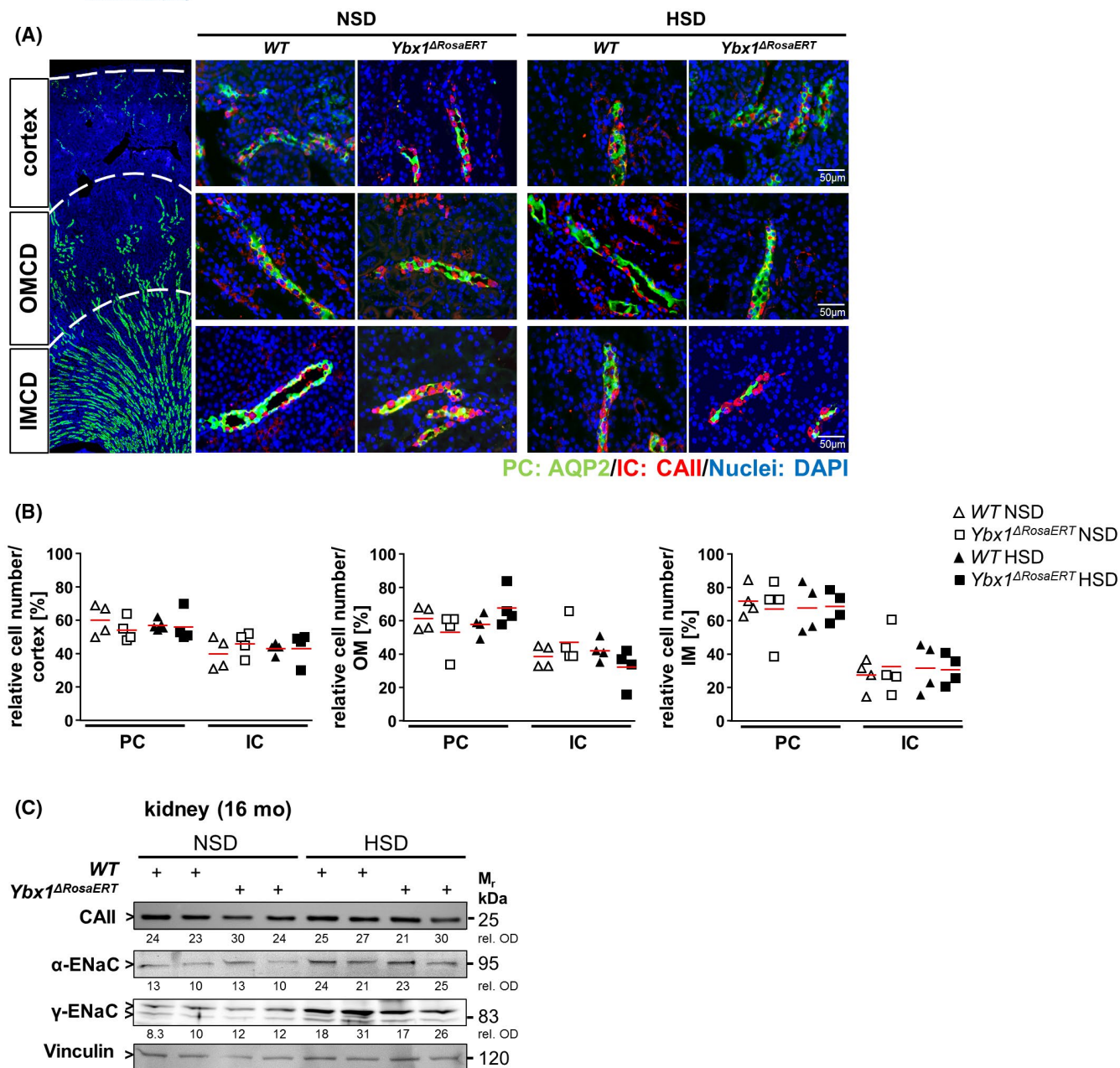


FIGURE 5 The depletion of *Ybx1* does not affect distal tubular function. (A) Illustration of the different kidney regions and collecting duct segments. Kidney sections of WT and *Ybx1* knockout mice were stained with antibodies directed against aquaporin-2 (AQP2) (green, PC marker) and CA11 (red, IC marker). Nuclei are visualized with DAPI. The cortex, outer medullary collecting ducts (OMCD), and the inner medullary collecting ducts (IMCD) are separated by the dashed white lines. Scale bars, 50 μ m. (B) The average percentage of PC and IC is depicted for the cortex, OMCD and IMCD. Y-box binding protein-1 is not required for maintenance of PC identity of the collecting ducts. Kidneys from *Ybx1* knockout mice after a 12-month observation period (NSD) shows no significant differences in the number of AQP2-expressing PC (green) and CA11-expressing IC (red) in comparison to WT mice. Moreover *Ybx1* knockout mice under HSD also show no differences to WT kidneys in the number of PC (green) and IC (red) in the three kidney compartments. ($n = 3$ mice per group, at least 100 cells were counted per collecting duct segment). (C) After 16 months on salt diets, kidneys were harvested and total proteins were extracted. Western blotting experiments for the main Na^+ transporters, namely α - and γ -ENaC were performed. Vinculin was taken as a loading control

deleted *Ybx1* after birth and therefore developmental influences of YB-1 are not observed, unless successive stress is applied, for example, to the skin. Kwon et al. showed that YB-1 plays an essential role in skin development and

regeneration.²⁶ In our model, the skin appears outwardly healthy, despite histological differences. A limitation is the mixed genetic background that may influence the susceptibility of mice to HSD.⁴⁹

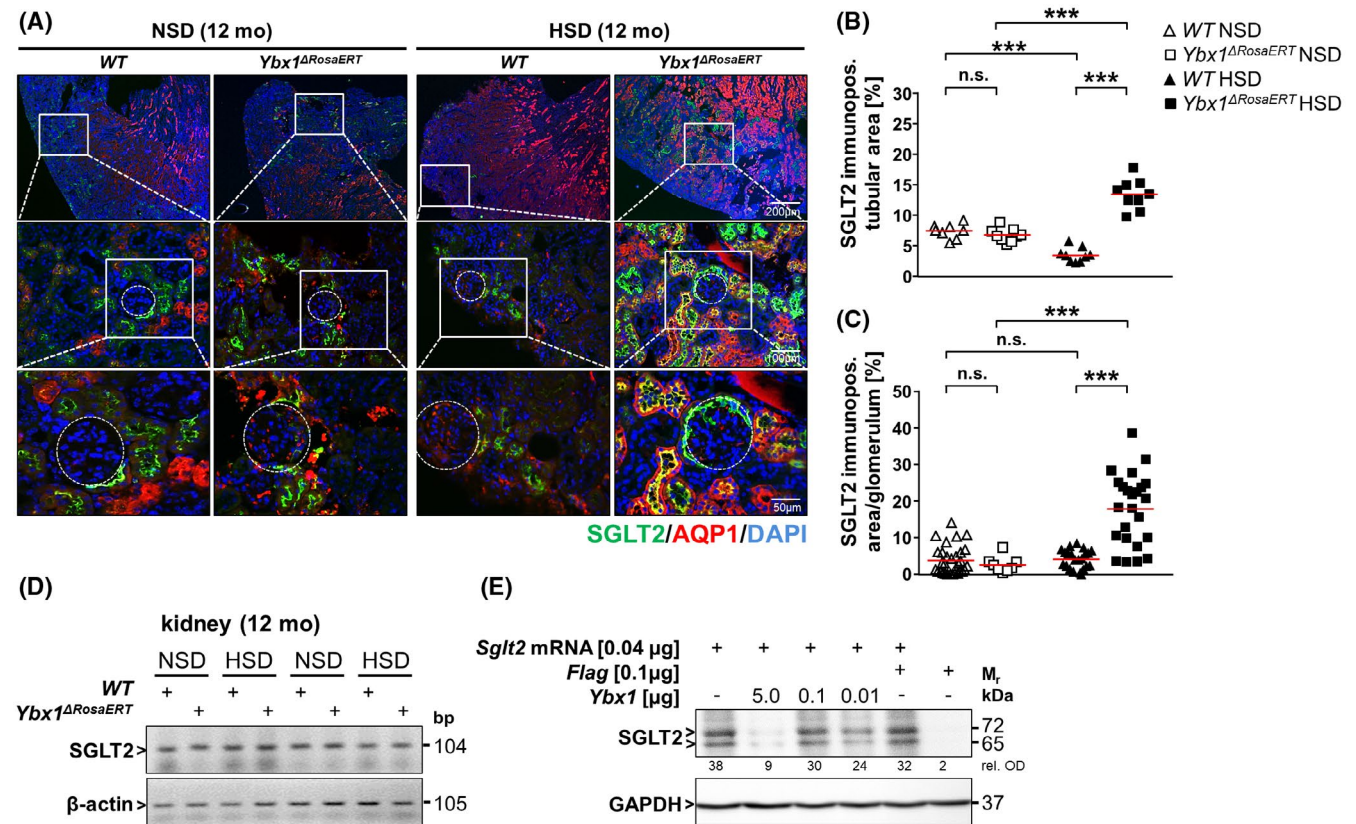


FIGURE 6 Y-box binding protein-1 (YB-1) translational represses *Sglt2*. (A) Kidney sections of WT and *Ybx1* knockout mice were stained with antibodies directed against AQP1 (red, proximal tubule marker) and sodium-glucose cotransporter-2 (SGLT2) (green). Nuclei are visualized with DAPI. Scale bars 200 and 50 μm. (B) Quantification of SGLT2 stained tissue [%]. The tubule and its surrounding positive staining fractions were analyzed using ImageJ software, with at least four mice per group. Data represent means ± SD, $n = 4$ for each group. (C) Quantification of SGLT2 stained glomeruli [%] analyzed using ImageJ software, with at least four mice per group. Data represent means ± SD, $n = 4$ for each group. (D) *Sglt2* transcripts in WT and *Ybx1* knockout kidneys under NSD and HSD. The *Sglt2* transcripts revealed no difference in expression levels, irrespective of the genotype. Both WT and *Ybx1* knockout organs showed corresponding bands of 104 bp. (E) YB-1 represses *Sglt2* mRNA translation. Western blot analysis of SGLT2 protein levels generated using an in vitro translation system. Biotinylated lysine was included to enable detection of the reaction product using streptavidin-HRP. To test the influence of YB-1 in the translation process, reactions were performed with or without the addition of recombinant YB-1 as indicated. The GAPDH loading control shows that equal amount of reticulocyte lysate were used in each reaction and that the reaction mix alone does not generate a product

The animals with no genetic depletion of *Ybx1*, glucosuria developed over time. One possible explanation to this development is the involvement of YB-1 in the translational regulation of the SGLT2 transcripts. *Sglt2* transcripts are regulated by SP1, HNF1α and HNF4α.⁵⁰ In vitro translation experiments confirm that YB-1 inhibits translation of *Sglt2* mRNA. Intake of 8% HSD for 24 weeks also leads to reduced SGLT2 expression of WT mice through the regulation of the PPARδ-SGLT2 pathway.⁴⁰ Zhao et al concluded that high sodium intake promotes urinary sodium excretion and glycosuria *via* increasing plasma adiponectin level through the activation of peroxisome proliferator-activated receptor delta (PPARδ). Enhanced adiponectin downregulates SGLT2, which in turn reduces reabsorption of sodium and glucose.⁴⁰ Interestingly, the tubules also show an inverted staining pattern, suggesting that tubular damage results in a loss

of membrane polarity^{51–53}; which fits to the loss of cell-cell contacts. The data suggest that *Ybx1*-deficient animals upregulate metabolite transporters in order to maintain homeostasis. SGLT2 is the transporter targeted by specific inhibitors that have proven protective for the kidneys with hyperglycemia (DECLARE, CREDENCE studies)^{54,55} as well as non-diabetic chronic kidney disease (DAPA-CKD study)⁵⁶ and proved to improve heart function, result in reduced blood pressure as well as decreased uric acid levels.⁵⁷ Our long-term salt exposure reveals a profound regulation of SGLT2 protein expression over time, and also the so-called phenomenon of glomerular tubularization.⁵⁸ Here, SGLT2 is expressed by cells with tubular phenotype residing at the inner layer of the Bowmans capsule at the site of parietal epithelial cells. The exact nature of these cells was not elucidated in the present study, however will be addressed in the future.

NHE3 is also present in proximal tubular cells, in order to maintain the balance between plasma and urinary Na^+ levels in response to HSD.⁵⁹ *Ybx1* knockouts show low levels of NHE3 suggesting that YB-1 also influence NHE3 expression. AQP1, the key regulator of water resorption in the proximal tubule, is reduced in WT HSD mice, but not in knockouts, supporting our hypothesis that YB-1 alters proximal tubular function. In CKD, the reabsorption of amino acids changes dynamically; at early stages urine levels are normal and in later stages excretion levels increase.⁶⁰ This is in line with our data, showing enhanced excretion levels within the urine of HSD mice. Despite the similarities with other tubular kidney diseases (ischemia/reperfusion injury and streptozotocin-induced nephropathy) reported for albuminuria, glucosuria, and amino aciduria,^{48,61,62} the effects on regulation of tubular transporters (cubulin, megalin, NHE3, SGLT2) appear to be unique to each model.⁴⁸ The urine content is further regulated in the distal tubules by specialized cell types. Although an upregulation of PC and reduction in IC is described for HSD,⁶³ we observed no such differences. We further observed that HSD mice develop excessive polyuria. This leads to the question of whether this is a physiological or pathological response to high salt intake. A pathological explanation could be that tubular cells are actively damaged by the high salt levels and no longer respond to ADH. On the other hand, one could explain this as a physiological response, whereby the resulting hypervolemia causes a reduction in renin release (negative feedback mechanism) and therefore reduced reabsorption of water within the collecting ducts. Alternatively, the increased volume of urine may be also be influenced by atrial natriuretic peptide (ANP), a diuretic hormone released from the heart in response to stretching of the atrium.⁶⁴ Furthermore, the expression of ENaC, known to be activated by aldosterone via the mineralocorticoid receptor,⁶⁵ increases following HSD. This is unexpected, because others have shown that HSD induces a tremendous decrease in γ -ENaC.⁶⁶ High sodium concentrations normally reduce aldosterone synthesis in the adrenal cortex resulting in less ENaC activity and therefore a decrease of renal Na^+ reabsorption.⁶⁷ In a study from Korte et al, a novel feedforward regulation of ENaC by sodium is described indicating that high sodium *per se* increases cellular ENaC, as well as abundance of functional plasma membrane ENaC.⁶⁸ Chronically administered high sodium concentrations do not increase ENaC transcription, but augment the cellular ENaC level and membrane abundance of the channel. Thus, they postulate that long-term, high sodium concentrations disturb the degradation of ENaC. These processes are independent of YB-1. Extending the observation period might reveal further influences, as cold shock proteins are expected to play a role in cell senescence.⁶⁹ Increasing the salt content to 8%

or switching to DOCA salt over a period of >18 months might incite elevated blood pressure. Finally, some effects of *Ybx1* deletion may be masked by the induction of *Ybx3* (DbpA), as these cold shock proteins share some cellular functions.^{70,71} However, it has recently been shown that HSD also effects the immune system.⁷² The data suggest that high salt intake induces the infiltration of immune cells into the kidney. The mechanisms mediating immune cell infiltration in the kidney are not well understood but probably associated with tissue damage. Our observations from the infiltrating immune cells will be followed up in the future to define the underlying pathomechanism of HSD, YB-1 and immune cell regulation.

In summary, we link long-term HSD with kidney damage, especially of the proximal tubules and pinpoint YB-1 as a key regulator of cell function and tubular transporter expression. Long-term loading with sodium chloride results in progressive damage of the kidney. Given the absent SGLT2 expression in WT animals it is conceivable that polyuria develops. In contrast, animals that lack YB-1 expression maintain SGLT2 expression and have less polyuria at 16 months.

ACKNOWLEDGMENTS

We are grateful to Lars Philipsen for performing MELC analysis, Mrs. Huß, Mrs. Heyer, Mrs. Königsmark, Mrs. Schuppe and Mrs. Weise for excellent technical assistance and to Prof. Vladimir Todorov for helpful discussion regarding renin expression in the kidney.

DISCLOSURES

N.E. is among the founders of NIPOKA, which will commercialize the podocyte exact morphology measurement procedure (PEMP). All other authors declare no competing interests.

AUTHOR CONTRIBUTIONS

Anja Bernhardt, Saskia Häberer, Sabine Brandt, JingJing Xu, Hannah Damerau, Johannes Steffen, Charlotte Reichardt, Katharina Wolters, Hannes Steffen, Berend Isermann, Katrin Borucki, Nadine Artelt, Nicole Endlich, Jonathan A Lindquist performed experiments and analyzed data. Renata Kozyraki provided essential reagents. Anja Bernhardt, Jonathan A. Lindquist, Peter R. Mertens wrote the manuscript. Peter R. Mertens conceived the study and supervised the work.

ORCID

Nicole Endlich  <https://orcid.org/0000-0001-6817-4099>

REFERENCES

1. Jantsch J, Schatz V, Friedrich D, et al. Cutaneous Na^+ storage strengthens the antimicrobial barrier function of the

- skin and boosts macrophage-driven host defense. *Cell Metab.* 2015;21:493-501.
2. Efsa Panel on Nutrition, Novel Foods and Food Allergens, Turck D, Castenmiller J, et al. Dietary reference values for sodium. *EFSA J.* 2019;17:e05778.
 3. WHO. *Guideline: Sodium Intake for Adults and Children.* World Health Organization; 2012. ISBN 978 92 4 150483 6.
 4. Meneton P, Jeunemaitre X, de Wardener HE, MacGregor GA. Links between dietary salt intake, renal salt handling, blood pressure, and cardiovascular diseases. *Physiol Rev.* 2005;85:679-715.
 5. Wenzel UO, Bode M, Kurts C, Ehmke H. Salt, inflammation, IL-17 and hypertension. *Br J Pharmacol.* 2019;176:1853-1863.
 6. Boero R, Pignataro A, Quarello F. Salt intake and kidney disease. *J Nephrol.* 2002;15:225-229.
 7. Kotchen TA, Cowley AW Jr, Frohlich ED. Salt in health and disease—a delicate balance. *N Engl J Med.* 2013;368:1229-1237.
 8. Verhave JC, Hillege HL, Burgerhof JGM, et al. Sodium intake affects urinary albumin excretion especially in overweight subjects. *J Intern Med.* 2004;256:324-330.
 9. Heerspink HL, Ritz E. Sodium chloride intake: is lower always better? *J Am Soc Nephrol.* 2012;23:1136-1139.
 10. Greger R. Physiology of renal sodium transport. *Am J Med Sci.* 2000;319:51-62.
 11. Dong W, Wang H, Shahzad K, et al. Activated protein C ameliorates renal ischemia-reperfusion injury by restricting Y-box binding protein-1 ubiquitination. *J Am Soc Nephrol.* 2015;26:2789-2799.
 12. Skälweit A, Doller A, Huth A, Kähne T, Persson PB, Thiele B-J. Posttranscriptional control of renin synthesis: identification of proteins interacting with renin mRNA 3'-untranslated region. *Circ Res.* 2003;92:419-427.
 13. Eliseeva IA, Kim ER, Guryanov SG, Ovchinnikov LP, Lyabin DN. Y-box-binding protein 1 (YB-1) and its functions. *Biochemistry/Biokhimiia.* 2011;76:1402-1433.
 14. Kohno K, Izumi H, Uchiumi T, Ashizuka M, Kuwano M. The pleiotropic functions of the Y-box-binding protein, YB-1. *BioEssays.* 2003;25:691-698.
 15. Lu ZH, Books JT, Ley TJ. YB-1 is important for late-stage embryonic development, optimal cellular stress responses, and the prevention of premature senescence. *Mol Cell Biol.* 2005;25:4625-4637.
 16. Lu ZH, Books JT, Ley TJ. Cold shock domain family members YB-1 and MSY4 share essential functions during murine embryogenesis. *Mol Cell Biol.* 2006;26:8410-8417.
 17. Zhang J, Zhao J, Jiang WJ, Shan XW, Yang XM, Gao JG. Conditional gene manipulation: cre-ating a new biological era. *J Zhejiang Univ Sci B.* 2012;13:511-524.
 18. Feng M, Whitesall S, Zhang Y, Beibel M, D'Alecy L, DiPetrillo K. Validation of volume-pressure recording tail-cuff blood pressure measurements. *Am J Hypertens.* 2008;21:1288-1291.
 19. Ding J, Kopchick JJ. Plasma biomarkers of mouse aging. *Age.* 2011;33:291-307.
 20. Li C, Hou S, Liu S, et al. The albumin-exendin-4 recombinant protein E2HSA improves glycemic control and beta-cell function in spontaneous diabetic KKAY mice. *BMC Pharmacol Toxicol.* 2017;18:48.
 21. Schock-Kusch D, Sadick M, Henninger N, et al. Transcutaneous measurement of glomerular filtration rate using FITC-sinistrin in rats. *Nephrol Dial Transplant.* 2009;24:2997-3001.
 22. Sahali D, Mulliez N, Chatelet F, et al. Comparative immunochemistry and ontogeny of two closely related coated pit proteins. The 280-kd target of teratogenic antibodies and the 330-kd target of nephritogenic antibodies. *Am J Pathol.* 1993;142:1654-1667.
 23. Artelt N, Siegerist F, Ritter AM, et al. Comparative analysis of podocyte foot process morphology in three species by 3D super-resolution microscopy. *Front Med.* 2018;5:292.
 24. Siegerist F, Ribback S, Dombrowski F, et al. Structured illumination microscopy and automatized image processing as a rapid diagnostic tool for podocyte effacement. *Sci Rep.* 2017;7:11473.
 25. Mehta S, McKinney C, Algie M, et al. Dephosphorylation of YB-1 is required for nuclear localisation during G2 phase of the cell cycle. *Cancers (Basel).* 2020;12:315.
 26. Kwon E, Todorova K, Wang J, et al. The RNA-binding protein YBX1 regulates epidermal progenitors at a posttranscriptional level. *Nat Commun.* 2018;9:1734.
 27. Hohlfeld R, Brandt S, Bernhardt A, et al. Crosstalk between Akt signaling and cold shock proteins in mediating invasive cell phenotypes. *Oncotarget.* 2018;9:19039-19049.
 28. Zhu C, Sauter E, Schreiter A, et al. Cold shock proteins mediate GN with mesangioproliferation. *J Am Soc Nephrol.* 2016;27:3678-3689.
 29. Kurtz A. Control of renin synthesis and secretion. *Am J Hypertens.* 2012;25:839-847.
 30. Graffe CC, Bech JN, Pedersen EB. Effect of high and low sodium intake on urinary aquaporin-2 excretion in healthy humans. *Am J Physiol Renal Physiol.* 2012;302:F264-F275.
 31. Loffing J, Loffing-Cueni D, Macher A, et al. Localization of epithelial sodium channel and aquaporin-2 in rabbit kidney cortex. *Am J Physiol Renal Physiol.* 2000;278:F530-F539.
 32. Weyer K, Storm T, Shan J, et al. Mouse model of proximal tubule endocytic dysfunction. *Nephrol Dial Transplant.* 2011;26:3446-3451.
 33. Ledoussal C, Lorenz JN, Nieman ML, Soleimani M, Schultheis PJ, Shull GE. Renal salt wasting in mice lacking NHE3 Na⁺/H⁺ exchanger but not in mice lacking NHE2. *Am J Physiol Renal Physiol.* 2001;281:F718-F727.
 34. Staruschenko A. Regulation of transport in the connecting tubule and cortical collecting duct. *Compr Physiol.* 2012;2:1541-1584.
 35. Mukherjee M, deRiso J, Otterpohl K, et al. Endogenous notch signaling in adult kidneys maintains segment-specific epithelial cell types of the distal tubules and collecting ducts to ensure water homeostasis. *J Am Soc Nephrol.* 2019;30:110-126.
 36. Tabatabai NM, North PE, Regner KR, Kumar SN, Duris CB, Blodgett AB. De novo expression of sodium-glucose cotransporter SGLT2 in Bowman's capsule coincides with replacement of parietal epithelial cell layer with proximal tubule-like epithelium. *J Membr Biol.* 2014;247:675-683.
 37. Farquhar WB, Edwards DG, Jurkowitz CT, Weintraub WS. Dietary sodium and health: more than just blood pressure. *J Am Coll Cardiol.* 2015;65:1042-1050.
 38. Hucke S, Eschborn M, Liebmann M, et al. Sodium chloride promotes pro-inflammatory macrophage polarization thereby aggravating CNS autoimmunity. *J Autoimmun.* 2016;67:90-101.
 39. Hosohata K, Yoshioka D, Tanaka A, Ando H, Fujimura A. Early urinary biomarkers for renal tubular damage in spontaneously hypertensive rats on a high salt intake. *Hypertens Res.* 2016;39:19-26.

40. Zhao Y, Gao P, Sun F, et al. Sodium intake regulates glucose homeostasis through the PPARdelta/adiponectin-mediated SGLT2 pathway. *Cell Metab.* 2016;23:699-711.
41. Titze J. A different view on sodium balance. *Curr Opin Nephrol Hypertens.* 2015;24:14-20.
42. Rakova N, Juttner K, Dahlmann A, et al. Long-term space flight simulation reveals infradian rhythmicity in human Na(+) balance. *Cell Metab.* 2013;17:125-131.
43. Tikellis C, Pickering RJ, Tsorotes D, et al. Activation of the Renin-Angiotensin system mediates the effects of dietary salt intake on atherogenesis in the apolipoprotein E knockout mouse. *Hypertension.* 2012;60:98-105.
44. Yu Q, Larson DF, Slayback D, Lundeen TF, Baxter JH, Watson RR. Characterization of high-salt and high-fat diets on cardiac and vascular function in mice. *Cardiovasc Toxicol.* 2004;4:37-46.
45. du Cailar G, Ribstein J, Mimran A. Dietary sodium and target organ damage in essential hypertension. *Am J Hypertens.* 2002;15:222-229.
46. Ohta Y, Tsuchihashi T, Kiyohara K, Oniki H. High salt intake promotes a decline in renal function in hypertensive patients: a 10-year observational study. *Hypertens Res.* 2013;36:172-176.
47. Amsellem S, Gburek J, Hamard G, et al. Cubilin is essential for albumin reabsorption in the renal proximal tubule. *J Am Soc Nephrol.* 2010;21:1859-1867.
48. Figueira MF, Castiglione RC, de Lemos Barbosa CM, et al. Diabetic rats present higher urinary loss of proteins and lower renal expression of megalin, cubilin, CIC-5, and CFTR. *Physiol Rep.* 2017;5:e13335.
49. Lantelme P, Rohrwasser A, Gociman B, et al. Effects of dietary sodium and genetic background on angiotensinogen and Renin in mouse. *Hypertension.* 2002;39:1007-1014.
50. Takesue H, Hirota T, Tachimura M, Tokashiki A, Ieiri I. Nucleosome positioning and gene regulation of the SGLT2 gene in the renal proximal tubular epithelial cells. *Mol Pharmacol.* 2018;94:953-962.
51. Molitoris BA, Wagner MC. Surface membrane polarity of proximal tubular cells: alterations as a basis for malfunction. *Kidney Int.* 1996;49:1592-1597.
52. Molitoris BA, Chan LK, Shapiro JI, Conger JD, Falk SA. Loss of epithelial polarity: a novel hypothesis for reduced proximal tubule Na⁺ transport following ischemic injury. *J Membr Biol.* 1989;107:119-127.
53. Molitoris BA, Falk SA, Dahl RH. Ischemia-induced loss of epithelial polarity. Role of the tight junction. *J Clin Invest.* 1989;84:1334-1339.
54. Perkovic V, Jardine MJ, Neal B, et al. Canagliflozin and renal outcomes in type 2 diabetes and nephropathy. *N Engl J Med.* 2019;380:2295-2306.
55. Kluger AY, Tecson KM, Lee AY, et al. Class effects of SGLT2 inhibitors on cardiorenal outcomes. *Cardiovasc Diabetol.* 2019;18:99.
56. Wheeler DC, Stefansson BV, Batiushin M, et al. The dapagliflozin and prevention of adverse outcomes in chronic kidney disease (DAPA-CKD) trial: baseline characteristics. *Nephrol Dial Transplant.* 2020;35:1700-1711.
57. Vlotides G, Mertens PR. Sodium-glucose cotransport inhibitors: mechanisms, metabolic effects and implications for the treatment of diabetic patients with chronic kidney disease. *Nephrol Dial Transplant.* 2015;30:1272-1276.
58. Isaac J, Togel FE, Westenfelder C. Extent of glomerular tubularization is an indicator of the severity of experimental acute kidney injury in mice. *Nephron Exp Nephrol.* 2007;105:e33-40.
59. Bobulescu IA, Moe OW. Luminal Na(+)/H(+) exchange in the proximal tubule. *Pflugers Arch.* 2009;458:5-21.
60. Durantou F, Lundin U, Gayraud N, et al. Plasma and urinary amino acid metabolomic profiling in patients with different levels of kidney function. *Clin J Am Soc Nephrol.* 2014;9:37-45.
61. Ansermet C, Centeno G, Lagarrigue S, et al. Renal tubular arginase-2 participates in the formation of the corticomedullary urea gradient and attenuates kidney damage in ischemia-reperfusion injury in mice. *Acta Physiol.* 2020;229:e13457.
62. Tojo A, Onozato ML, Ha H, et al. Reduced albumin reabsorption in the proximal tubule of early-stage diabetic rats. *Histochem Cell Biol.* 2001;116:269-276.
63. Humphreys BD. Mapping kidney cellular complexity. *Science.* 2018;360:709-710.
64. Theilig F, Wu Q. ANP-induced signaling cascade and its implications in renal pathophysiology. *Am J Physiol Renal Physiol.* 2015;308:F1047-F1055.
65. Zaika O, Mamenko M, Staruschenko A, Pochynyuk O. Direct activation of ENaC by angiotensin II: recent advances and new insights. *Curr Hypertens Rep.* 2013;15:17-24.
66. Udwan K, Abed A, Roth I, et al. Dietary sodium induces a redistribution of the tubular metabolic workload. *J Physiol.* 2017;595:6905-6922.
67. Stockand JD. New ideas about aldosterone signaling in epithelia. *Am J Physiol Renal Physiol.* 2002;282:F559-F576.
68. Korte S, Strater AS, Druppel V, et al. Feedforward activation of endothelial ENaC by high sodium. *FASEB J.* 2014;28:4015-4025.
69. Xiao YZ, Yang M, Xiao Y, et al. Reducing hypothalamic stem cell senescence protects against aging-associated physiological decline. *Cell Metab.* 2020;31(534-548):e535.
70. Lyabin DN, Eliseeva IA, Smolin EA, et al. YB-3 substitutes YB-1 in global mRNA binding. *RNA Biol.* 2020;17:487-499.
71. Lindquist JA, Mertens PR. Cold shock proteins: from cellular mechanisms to pathophysiology and disease. *Cell Commun Signal: CCS.* 2018;16:63.
72. Jobin K, Muller DN, Jantsch J, Kurts C. Sodium and its manifold impact on our immune system. *Trends Immunol.* 2021;42:469-479.

SUPPORTING INFORMATION

Additional Supporting Information may be found online in the Supporting Information section.

How to cite this article: Bernhardt A, Häberer S, Xu J, et al. High salt diet-induced proximal tubular phenotypic changes and sodium-glucose cotransporter-2 expression are coordinated by cold shock Y-box binding protein-1. *FASEB J.* 2021;35:e21912. <https://doi.org/10.1096/fj.20210667RR>